J. COMBIN. MATH. COMBIN. COMPUT. 127b (2025) 6823--6848

Journal of Combinatorial Mathematics and Combinatorial Computing
www.combinatorialpress.com/jcmcc

Combinatorial Press

Research on fine structure characteristics of construction asphalt mixtures based on image processing algorithms

Haocheng Xiong[1,✉], Haowen Zheng[1]

[1] *School of Civil and Resources Engineering, University of Science and Technology, Beijing, 100083, China*

ABSTRACT

Asphalt mixture is a multiphase composite material composed of aggregates, asphalt, fillers and other materials of different properties, in which the coarse aggregate forms the main bearing structure, and the fine aggregate fills the voids formed by the coarse aggregate to improve the structural stability. In this paper, computerized tomography is used to obtain the preliminary tomographic images of asphalt mixture specimens, and the image is effectively segmented through the grayscale thresholding method, and the scanning results are refined. Using voxel-based three-dimensional reconstruction method, the three-dimensional finite element model of asphalt mixture is reconstructed, and the corresponding fine structural characterization index is proposed to prepare asphalt mixture specimens and study the fine structural characteristics of asphalt mixture. The distribution characteristics of the contact connectivity tree of the asphalt mixture are analyzed, with 61.54% of the primary and middle order trees in gradation 1, 92.31% in gradation 2, 83.33% in gradation 3 and 58.82% in gradation 4. It shows that the higher the percentage of second-order connectivity tree, the worse the skeleton contact connectivity, which is not conducive to the improvement of asphalt mixture shear strength. For the four different gradation specimen slice images, the generated areas of each order tree were statistically analyzed. Most of the primary order tree areas were distributed between 100 mm²-300 mm², the intermediate order tree areas were basically distributed between 200 mm²-400 mm², and the high order trees were distributed between 400 mm²-500 mm². The area distribution of high-order tree of grade 4 is more uniform and concentrated, which has better load transfer chain and rutting resistance.

Keywords: Computed tomography, Gray scale threshold method, Three-dimensional finite element model, Load transfer chain, Asphalt mixture specimen

✉ Corresponding author.
E-mail address: 13071130135@163.com (H. Xiong).
Received 01 February 2024; Revised 20 April 2024; Accepted 10 November 2024; Published Online 16 April 2025.
DOI: 10.61091/jcmcc127b-373

1. Introduction

Since the 21st century, all kinds of infrastructure has made rapid development, asphalt mixture as the world's most widely used paving materials, with short construction period, waterproof, leveling, high comfort, anti-corrosion protection and other advantages [1-3]. Under the action of complex loading and hydrogeological environment, asphalt surface is prone to cracking, fatigue and other diseases, which seriously shorten the service life of asphalt surface, in order to improve the durability of asphalt surface, it is necessary to put forward higher requirements for asphalt mixture material design and composition optimization [4-7]. The service performance of asphalt mixtures is not only related to the multiphase nature of the material composition, but also related to its granular material properties on the fine-macroscopic scale [8-9]. The macroscopic mechanical properties of asphalt mixtures originate from their fine particle interaction behavior. Asphalt mixture strength is mainly composed of friction and embeddedness between aggregate particles, as well as the asphalt-aggregate bond [10]. Plastic deformation is mainly formed by aggregate particles-mortar flow [11]. Cracks develop mainly from microdamage between aggregate particles [12]. Water damage is mainly caused by asphalt spalling on the surface of aggregate particles [13]. Thus, the mechanical properties of asphalt mixtures are closely related to aggregate particle gradation, mortar, and fine-scale parameters between particle-mortar interfaces.

Traditional asphalt mixture design methods have certain limitations in establishing the relationship between the internal structure and composition of asphalt mixtures and the macroscopic mechanical properties, and they also have greater limitations in revealing the local damage damage mechanism due to the non-uniform nature of the material [14-17]. Only by studying the asphalt mixtures with complex fine structure can we fundamentally solve the applicability problems in engineering. In addition, asphalt mixture belongs to the aggregate-mortar-void three-phase structural body, in which the mineral mixture accounts for more than 90% of the mass and 85% of the volume, which is the main source of strength of asphalt mixture, and has a significant impact on the service performance of asphalt mixtures, which have the typical properties of bulk particulate matter [18-20]. However, asphalt mixture is a complex multiphase composite material containing various components such as aggregate, asphalt, mineral powder and additives, and the complexity of the material composition and the limitations of the research methodology have led to the current unclear relationship between the material composition and the fine structure [21-22]. On the other hand, the fine structure characteristics of asphalt mixtures have a direct impact on their macroscopic properties, while macroscale studies are difficult to mechanistically explain the complex damage behavior of asphalt mixtures [23]. Therefore, it is necessary to carry out in-depth research on the fine structure of asphalt mixtures to break through the limitations of macro-scale research methods. And with the deep development of digital image technology, the use of algorithms such as image segmentation, data capture, deep learning and other algorithms, through the digitization, enhancement, restoration, segmentation and recognition of images, has brought a turnaround in the solution of these problems [24].

In this paper, X-ray CT instrument is used to obtain the tomographic image of asphalt mixture specimen, and the operation method of corrosion followed by expansion is used to eliminate the small stray particles in the aggregate region, and image segmentation is carried out by using the threshold method for the gray scale contrast. Based on the cone-beam filtering inverse projection algorithm, the tomographic images obtained from X-ray CT were used to reconstruct the asphalt mixture in three dimensions, and construct a three-dimensional finite element model of the scanned asphalt mixture image. From the five aspects of shape, angularity, distribution characteristics, contact characteristics and uniformity, the three-dimensional fine structure characterization evaluation indexes of aggregates are proposed. SMA-16 gradation is selected, and the specimens are prepared by using the same morphological characteristics of aggregates, and then the fine structure characterization experiments of asphalt mixtures are carried out.

2. Research on fine structure of construction asphalt mixtures based on image processing

2.1. CT technology

2.1.1. Basic Components of a CT. Computed tomography (CT) technology was born in 1971 and was first used in medicine. Because of its "see-through" characteristics, it has been emphasized by researchers in various fields. Since the end of the 1990s, computed tomography has been gradually applied to the study of the internal microstructure of asphalt mixtures. Nowadays, high-precision industrial CT has become one of the important means to obtain the internal tomographic images of materials. There are many research organizations in China that have advanced X-ray CT scanning systems. Due to the different needs of users, there are big differences in the configuration of X-ray CT parameters, but the basic structure and data flow are largely the same.

In this paper, the AX-5000CT open commercial precision industrial CT of AOI Precision Instruments (Shanghai) Co., Ltd. is used to obtain the tomographic images of asphalt mixture specimens, and this paper is based on the cone-beam filtering inverse projection algorithm for three-dimensional reconstruction of the tomographic images obtained from the asphalt mixture [25].

2.1.2. CT imaging principles. An X-ray CT system is a device that utilizes the large amount of ray absorption data obtained when scanning around a subject to reconstruct its tomographic image. When the $X-ray$ rays emitted by the $X-ray$ tube are collimated by a collimator, they pass through the object under test in the form of a narrow beam and are received by a detector. The detector performs photoelectric conversion and converts the received optical signal into an electrical signal. It is then converted into a digital signal by an analog/digital converter and input into a computer for digital processing. The selected level is divided into a number of rectangular bodies of the same volume, i.e., voxels, and the $X-ray$ attenuation coefficient of each voxel is calculated and arranged into a digital matrix. The digital matrix is then converted by a digital/analog converter to pixels of different grayscale, and these pixels of different grayscale are arranged in a matrix to form a CT image.

For a homogeneous material, the attenuation process of the rays satisfies the Beer-Lambert law when a ray of initial intensity N_0 passes through its interior:

$$N = N_0 e^{-\mu L} \tag{1}$$

Where: N_0 intensity of the ray before incidence, N intensity of the ray when it passes through the object, μ attenuation coefficient of the material, L thickness of the material.

For non-homogeneous materials, the uneven distribution of density within the material leads to differences in the degree of attenuation of $X-ray$. In this case, the intensity of the ray after passing through each component satisfies equations (2), (3) and (4).

When a monoenergetic $X-ray$ ray beam passes through a non-homogeneous material, the process of calculating the ray intensity is as follows:

$$N_1 = N_0 e^{-\mu_1 l} \tag{2}$$

$$N_2 = N_1 e^{-\mu_2 l} \tag{3}$$

$$\ldots\ldots$$

$$N_n = N_{n-1} e^{-\mu_n l} \tag{4}$$

The formula for calculating the light intensity of a monoenergetic $X-ray$ ray beam after passing through a non-homogeneous material is obtained after superposition:

$$N_n = N_0 e^{-(\mu_1+\mu_2+\cdots+\mu_n)l} \tag{5}$$

Obtained by taking logarithms on both sides of Eq. (5):

$$(\mu_1+\mu_2+\cdots+\mu_n)l = \ln\frac{N_0}{N_n} \tag{6}$$

Equation (6) is obtained by deformation:

$$(\mu_1+\mu_2+\cdots+\mu_n)l = \frac{1}{l}\ln\frac{N_0}{N_n} = p \tag{7}$$

P is the projection of the material in the ray direction. Eqs. (5) and (7) can be written in integral form when the chosen cell size is small enough:

$$N = N_0 e^{-\int \mu(l)dl} \tag{8}$$

$$p = \ln\frac{N_0}{N} = \int \mu(l)dl \tag{9}$$

When the projection P of a material in the same plane, along any straight line is known, the Radon transform can be used to reconstruct the projection into the image of the material in space, this theory establishes a bridge between the results of different projections and the reconstruction of the spatial image.

The attenuation coefficients of the different components of a material's interior to $X-ray$ are characterized by the CT value, which reflects the difference in density of the different components, and the higher the density, the higher the CT value.Hounsfield defines the CT numbers of air and water as 0 and -1000, respectively.

Eq. (10) is the CT value calculated as:

$$n_{CT} = \frac{\mu-\mu_w}{\mu_w}\times 1000 \tag{10}$$

Where: μ is the attenuation coefficient of the measured object to the ray, and μ_w is the attenuation coefficient of water to the ray.

2.2. Digital Image Processing Technology

There are many problems in the image results from X-ray CT scanning, which directly affect the accuracy of the 3D finite element model. In order to truly characterize the fine structure of asphalt mixtures, the scanning results are refined in this paper.

2.2.1. Asphalt Mixture Image Enhancement. Due to the inhomogeneity of the material and $X-ray$ CT scanning accuracy problems, the resulting image has different material boundary areas are not obvious, the same material within the noise and so on, this will seriously affect the material differentiation and three-dimensional modeling, so the need for image optimization processing.

VGStudio software provides some basic image processing functions, of which erosion and expansion are common morphological operations. Erosion is used to remove certain pixels from the boundaries of an image object, while expansion adds pixels to the object boundaries.

In morphological transformations, erosion merges two sets merged by vector subtraction:

$$X - B = \{p \in \varepsilon^2, p+b \in X, \forall b \in B\} \tag{11}$$

The expansion uses vector addition:

$$X + B = \{p \in \varepsilon^2, p = x + b, x \in X, b \in B\} \tag{12}$$

Aiming at the characteristics of the image obtained from scanning reconstruction, the operation method of corrosion followed by expansion is adopted in order to eliminate the small stray particles in the aggregate area and smooth the contact boundary between the aggregate and asphalt mortar without significantly changing the area of the aggregate or asphalt mortar area. After repeated tests, two corrosion and expansion operations in sequence can obtain better results.

The processed two-dimensional image still exists that the boundary of aggregate and mortar is not obvious enough, after repeated attempts and tests, the median filtering of the image by applying the 9×9 template can get the desired effect. Median filtering operation is a nonlinear image processing method, which can remove the noise well and also protect the edge region of the target image from being affected, and it is mainly based on the result of sorting the pixels in the object region according to the grayscale to decide the grayscale of the center pixel, which can be realized by Matlab software:

$$g(x, y) = median\{f(x-i, y-i)\} \tag{13}$$

2.2.2. Trinomialization of asphalt mixture tomography images. Asphalt mixture can be regarded as a mixture composed of aggregate, asphalt mortar and void structure together, due to the three materials density exists a big difference, by X-ray CT scanning and image processing presents different gray scale, the difference in gray scale to determine the threshold value can be better material differentiation.

Thresholding method is a more convenient and effective segmentation algorithm for images with more obvious gray scale contrast, the principle of which is to use the difference in gray scale value between the target and the background in the image that needs to be segmented, and divide the image into two or more gray scale regions according to the demand by selecting the appropriate threshold value. Therefore, determining the grayscale threshold between aggregate, asphalt mortar and voids becomes the key to be able to segment effectively.

2.3. Research on 3D model reconstruction algorithm

2.3.1. Principles of 3D Model Reconstruction. The 3D visualization model is not directly used for numerical simulation, so it is necessary to explore the method of establishing 3D finite element models based on CT scan images for subsequent research work.

The essence of three-dimensional reconstruction of asphalt mixture is to superimpose n consecutive two-dimensional tomographic images obtained after CT scanning, and the smaller the spacing between two adjacent images, the more accurate the model obtained, and the image processing software such as VG Studio, ImagePro Plus, and IDL are all based on this principle of three-dimensional visualization and reconstruction.

The 3D reconstruction methods of asphalt mixture fine structure can be roughly categorized into two kinds, based on the outer surface and based on voxels. The outer surface-based 3D reconstruction method reconstructs the surface by setting a set of parallel contour lines, which can minimize the amount of data, but has a low correlation with the resolution of the original image. The voxel-based 3D reconstruction method has higher accuracy and reliability by constructing units on the surface of each material solid contour that are connected to form the surface of the solid, but it occupies a large amount of storage space and affects computational efficiency.

The ideal 3D model of fine structure of asphalt mixtures should facilitate the later calculation as well as accurately reflect the fine features of the structure, and there is an essential contradiction between reducing the number of units and reducing the error. Therefore, how to choose the 3D reconstruction method to achieve a balance between the two is particularly important [26].

2.3.2. 3D Model Reconstruction Algorithm:

1) Cell and node numbering. Figure 1 shows the unit and node numbering of the first CT grayscale image, each pixel point of the 2D CT grayscale image is regarded as a unit, and each unit is surrounded by four nodes, and the units and nodes are numbered sequentially from the first image from left to right, and from top to bottom, respectively. Assuming $m \times n$ pixels, the cells are numbered from 1 to mn and the nodes are numbered from 1 to $(m+1)(n+1)$.

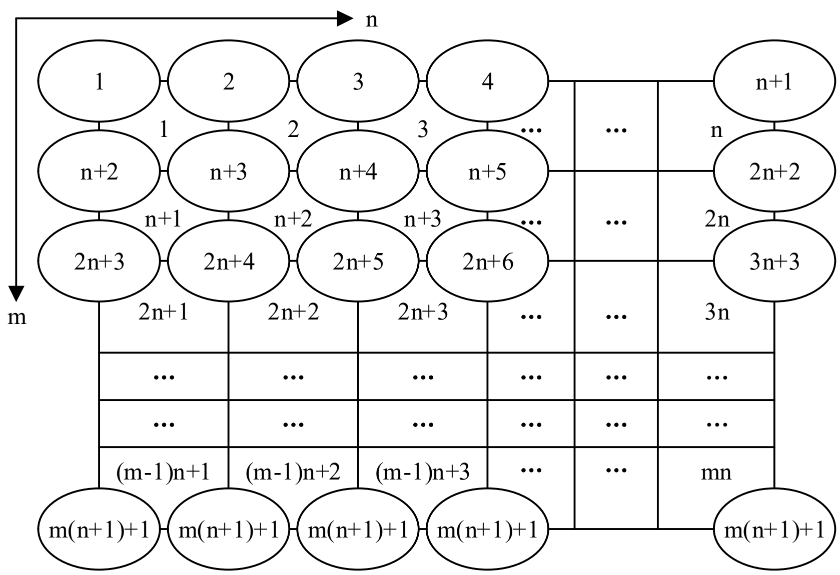

Fig. 1. The first CT gray image unit and node number

2) Determine the relationship between the unit and the eight surrounding nodes. Each three-dimensional hexahedral unit is surrounded by eight neighboring nodes, based on the syntax rules of the input file in Abaqus, it is necessary to find the logical relationship between each unit and its eight neighboring points around it. According to the previous numbering rules, this function can be easily realized.

3) Determine the three-dimensional coordinates of the nodes. According to the actual size of the specimen and the pixel accuracy of the CT scan image, the three-dimensional coordinates of each node can be determined, so that each unit can be localized.

4) Extraction of units in the mixing area. For the image obtained by CT scanning, it contains the mixture area and the background area, and it is necessary to extract the units in the mixture area. Here we can use the pointer method, that is, the center of the specimen as the center of a circle, a certain radius of the circle, the unit within the circle that is the unit in the mixture area. Considering the boundary effect in the process of specimen preparation, the radius is taken as 45mm, which is equivalent to the actual specimen coring.

5) Extraction of aggregates, asphalt mortar and voids. The unit numbers of aggregate, asphalt mortar and void are extracted by threshold segmentation method respectively.

6) Write input file. According to the syntax rules of Abaqus input file, the aggregate, asphalt mortar and void unit sets were input as parts in order to assign different material properties. Thus, a three-dimensional finite element model of asphalt mixture considering the fine structure is obtained, which lays the foundation for future numerical simulations.

3. Research on the characterization method of three-dimensional fine structure of asphalt mixtures

3.1. *Shape indicators*

The shape characteristics of aggregate can be evaluated by the shape index F_1, shape factor F_2 and the ratio of two parameters K between the three axes of aggregate length, width and height. Among them, the shape index F_1 is a two-dimensional index, the shape factor F_2 and the ratio of axial lengths K are three-dimensional indexes, and the calculation formulas of the three are shown in Eqs. (14), (15) and (16). F_1 is a value of ≥ 1, when $F_1 = 1$, the aggregate two-dimensional projection surface is circular, and the larger F_1 is, the more it indicates that the aggregate two-dimensional projection surface deviates from the circular and is close to the needle. When $F_2 = 1$, the shape of aggregate is sphere or square cube, when $F_2 < 1$, the aggregate is close to needle-like, when $F_2 > 1$, the aggregate is close to sheet-like. K is a value of ≥ 1, and the larger K is, the closer the aggregate is to needle-like flakes:

$$F_1 = \frac{C \times C}{4 \times \pi \times S} \tag{14}$$

$$F_2 = \frac{T \times L}{W^2} \tag{15}$$

$$K = \frac{L}{W} \tag{16}$$

where: F_1 is the shape index of the aggregate, C is the perimeter of the two-dimensional projection surface of the aggregate, S is the area of the two-dimensional projection surface of the aggregate, F_2 is the shape factor of the aggregate, L is the longest axis of the aggregate, W is the sub-major axis of the aggregate, that is, the particle size of the aggregate, T is the minor axis of the aggregate, and K is the ratio of the long axis of the aggregate to the particle size of the aggregate.

3.2. *Angularity indicators*

The angularity feature of the aggregate can be characterized by the offset value between it and the equivalent smooth contour with the same volume parameter. For the 2D cross-sectional image of the aggregate, the equivalent smooth contour can be taken as a circle with the same area or an ellipse with the same standard second-order central moment. For the three-dimensional model of the aggregate, the angularity of the aggregate can be evaluated by the sphericity of the aggregate, which is the ratio of the surface area of the sphere with the same volume of the aggregate to the actual surface area of the aggregate, and since the surface area of the aggregate is difficult to be determined accurately, it is often approximated and solved by the three principal axes dimensions of the aggregate in the previous studies, which is calculated in Equation (17). The approximate solution method of sphericity based on the axial lengths of aggregate particles does not sufficiently consider the variability of the aggregate in local angularity, and at the same time, taking the sphere as the equivalent smooth contour, it is not able to better exclude the interference of the shape of the aggregate on the results of the calculation of the angularity of the aggregate, so it is actually still a kind of shape index:

$$\psi = \frac{\left(\frac{\pi}{6}LWT\right)^{\frac{1}{3}}}{\left(\frac{\pi}{6}L\right)^{\frac{1}{3}}} = \left(\frac{WT}{L^2}\right)^{\frac{1}{3}} \tag{17}$$

Where $\varPsi$ is the sphericity of aggregate, L is the longest axis of aggregate, W is the second longest axis of aggregate, i.e., aggregate grain size, and T is the short axis of aggregate.

3.3. Distributional Characterization Indicators

Aggregate tilt angle can describe the arrangement direction of aggregate in asphalt mixture, and also can reflect the compaction state during the specimen molding process to a certain extent, so the aggregate tilt angle can be used to characterize the distribution of aggregate in asphalt mixture. In the analysis of aggregate inclination angle of two-dimensional cross-section image, usually take the line between the two farthest points on the boundary of aggregate particles, i.e., the main axis of the aggregate, and define the angle between the main axis of the aggregate and the horizontal coordinate system as the angle of aggregate inclination.

Assuming that the right-angle coordinates of the endpoints on both sides of the spindle are (x_1, y_1) and (x_2, y_2) respectively, the formula for calculating the aggregate inclination angle α is shown in equation (18):

$$\alpha = \arctan\left(\frac{y_2 - y_1}{x_2 - x_1}\right) \tag{18}$$

Where α is the angle of inclination of the two-dimensional cross-section of the aggregate with respect to the horizontal direction, x_1 is the transverse coordinate of the spindle endpoint 1, y_1 is the longitudinal coordinate of the spindle endpoint 1, x_2 is the transverse coordinate of the spindle endpoint 2, and y_2 is the longitudinal coordinate of the spindle endpoint 2.

The tilt angle α of the aggregate of a 2D section is generally taken in the range of $[-90, 90]$ to distinguish the degree of tilt of the long axis of the aggregate along the x-axis in the positive direction and the negative direction, and when $\alpha = 0°$, the aggregate is completely flat and when $\alpha = \pm 90°$, the aggregate is completely flat. circ}}$$, the aggregate is upright with respect to the horizontal direction. In the past research, because only can extract the aggregate tilt angle of a certain or several two-dimensional cross sections of asphalt mixture specimens, the analysis of the aggregate tilt angle only has statistical significance for the distribution characteristics of multiple aggregates, and the two-dimensional cross-section projection of three-dimensional aggregate particles in the horizontal direction, the degree of tilt does not have any practical significance for the distribution characteristics of a single aggregate in the three-dimensional space.

In order to obtain the inclination degree and distribution characteristics of aggregates in three-dimensional space, this paper develops a method for calculating the inclination angle of aggregates based on the three-dimensional aggregate particle model, which defines the line between the two farthest points on the particle aggregate boundary as the long axis of the aggregate, and establishes the local coordinate system xyz with the vertex on one side of the element of the 3D structure matrix of the aggregate as the origin, the column direction of the matrix as the x axis, the row direction of the matrix as the y axis, and the page direction of the matrix as the z axis. The angle between the long axis of the aggregate and the three axes of x, y, z is the inclination angle of the aggregate, as shown in Figure 2, and the implementation method is briefly described as follows.

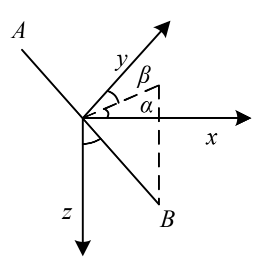

Fig. 2. Aggregate three-dimensional space inclination Angle

1) Generation of a 3D structure matrix of a single aggregate by means of an extraction program for 3D aggregate particles.
2) Extract the boundary convex hull points of the aggregate through the convhull function.
3) Traverse the points on the convex hull and calculate the distance between two points on the boundary convex hull.
4) Take the maximum value of the distance between two points, which is the long axis L of the aggregate.
5) Extract the endpoints on both sides of the long axis L, compute the long axis vector, and compute the angle between the long axis vector and the x, y, and z axes by the angle computation formula:

$$\alpha = \arccos\frac{a}{\sqrt{a^2+b^2+c^2}} \tag{19}$$

$$\beta = \arccos\frac{b}{\sqrt{a^2+b^2+c^2}} \tag{20}$$

$$\gamma = \arccos\frac{c}{\sqrt{a^2+b^2+c^2}} \tag{21}$$

where α is the angle between the long axis of the aggregate and the x-axis, β is the angle between the long axis of the aggregate and the y-axis, γ is the angle between the long axis of the aggregate and the z-axis, a is the x-directional component of the long axis vector of the aggregate, b is the y-directional component of the long axis vector of the aggregate, and c is the z-direction component of the aggregate long-axis vector.

Because the degree of aggregate inclination in the vertical direction can best reflect the distribution state and compaction degree of aggregate in asphalt mixture, this paper only adopts the angle between the aggregate and the z axis direction as the evaluation index of the distribution characteristics of the aggregate, and the inclination angle takes the value range of $[0,90]°$.

3.4. Indicators of contact characteristics

Under the assumption that only one contact point exists between two or two aggregates, the realization method is briefly described as follows.
1) Generate the 3D structure matrix of a single aggregate through the extraction program of 3D aggregate particles.
2) Traverse the three-dimensional structure matrix of the aggregate, extract the boundary convex hull points of the aggregate through the three-dimensional convex hull point extraction function, and extract the form center coordinates of the material particles.
3) Calculate the global coordinates of the boundary points of each aggregate particle and the shape center of the aggregate with respect to the 3D numerical matrix of the asphalt mixture.
4) Calculate the distance between the form centers of two aggregates, if the distance between the form centers is less than 1.5 times the sum of the particle diameters of the two aggregates, and the particle diameters of the two aggregates are ⩾4.75mm, then the next step of the calculation is carried out, otherwise, it is considered that there is no contact point between the two aggregates.
5) Traverse the three-dimensional structure matrix of the aggregate, calculate the distance of the boundary points between any two aggregates, and take the minimum value of the distance between the boundary points as the contact distance between the two aggregates.
6) Based on the contact threshold, calculate the number of contact points of aggregates in asphalt mixture.

3.5. Distribution uniformity index of aggregates

The uniformity evaluation method based on the static distance calculation formula is based on the idea of establishing a plane rectangular coordinate system with the midpoint of the two-dimensional cross-section image of the asphalt mixture specimen as the origin, and calculating the sum of static distances of all the aggregates on the current cross-section image as shown in Eqs. (22) and (23). Under the assumption that the aggregate is completely uniformly distributed in the plane, the sum of the static distances of the aggregates to the x-axis and the y-axis should be 0. Therefore, the degree to which the sum of the static distances is shifted by 0 is the degree of segregation of the aggregates distributed in the plane [27]:

$$S_x = \sum_{i=1}^{n} m_i \times x_i \tag{22}$$

$$S_y = \sum_{i=1}^{n} m_i \times y_i \tag{23}$$

Where S_x is the sum of the static distance of the aggregate image with respect to the x-axis, S_y is the sum of the static distance of the aggregate image with respect to the y-axis, m_i is the area of the aggregate image, x_i is the transverse coordinate of the center of form of the aggregate image, and y_i is the longitudinal coordinate of the center of form of the aggregate image.

With reference to this two-dimensional homogeneity evaluation index, this paper proposes a three-dimensional homogeneity evaluation index of aggregate particles, using the product of the volume of coarse aggregate and its form center coordinates to characterize the homogeneity of coarse aggregate in the direction of x axis, y axis, z axis, as shown in Eqs. (24), (25), and (26), respectively:

$$S_x = \sum_{i=1}^{n} v_i \times x_i \tag{24}$$

$$S_y = \sum_{i=1}^{n} v_i \times y_i \tag{25}$$

$$S_z = \sum_{i=1}^{n} v_i \times z_i \tag{26}$$

Where v_i is the volume of three-dimensional aggregate particles, S_z is the sum of static distances of aggregate images relative to the z axis.

In order to comprehensively consider the degree of uniformity of the mixture in the overall spatial distribution, the sum of the squares of the static distances of the aggregates in the three directions is calculated, at which time the distribution uniformity index of the coarse aggregate, i.e., the uniformity coefficient, is shown in Eq. (27):

$$S = \sqrt{S_x^2 + S_y^2 + S_z^2} \tag{27}$$

where S is the coarse aggregate homogeneity factor.

3.6. Asphalt Mixture Preparation

3.6.1. Gradation design. Fig. 3 is the median value of the recommended gradation of SMA-16, in order to verify the characteristics and discreteness of the three-dimensional mesoscopic structural parameters in the characterization of a specific type of asphalt mixture, the SMA-16 gradation is selected in this paper, and the aggregate with the same morphology characteristics is used to complete the preparation of the mixture specimen, in order to make the study representative, according to the Technical Code for Construction of Building Asphalt Pavement (JTG_F40-2017), the median gradation value of the recommended gradation is selected for gradation design. The SMA-16 gradation type decreases with decreasing pass rate at all pass rates except 26.5% and 19%, when the pass rate is 0.075%, SMA-16 is 10.5.

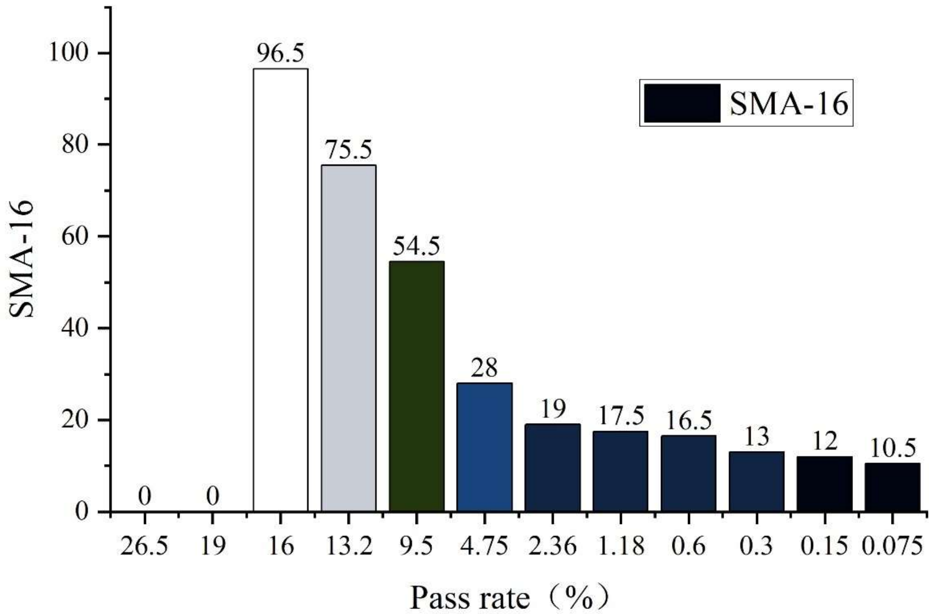

Fig. 3. SMA-16 recommendation grading

3.6.2. Specimen preparation. The aggregate type used in this paper is basalt and the mineral powder is limestone mineral powder, and its performance indexes are shown in Table 1 and Table 2.

Table 1. Asphalt mixture base nature energy indicator

Mesh size (mm)	16	13.2	9.5	4.75
Apparent density (g/cm^3)	2.8896	2.8152	2.8366	2.8321
Capillary density (g/cm^3)	2.8369	2.8366	2.7659	2.6321
Water absorption rate (%)	0.0578	0.0245	0.9978	2.5978

Table 2. Mineral energy index

Index parameter	Test result	Specification requirement
Apparent density	2.5985	⩾2.5
Moisture content	0.4366	⩽1
Drainage number	0.7856	<1
Plasticity index	2.9985	<4

The asphalt is a high viscosity and high elasticity modified asphalt, and its performance index is shown in Table 3. The amount of asphalt was 5.6%, and lignin fiber, which accounted for 0.3% of the total asphalt mixture, was added. The molding method is rotary compaction, and the diameter of the mixture specimen is 101.6 mm. In order to ensure the consistency of the molded asphalt mixture specimens under different aggregate morphology conditions, the height of 100 mm after compaction is uniformly adopted as the compaction standard.

Table 3. Basic performance index of high viscosity and high elasticity modified asphalt

Index parameter	Test result	Unit
Penetration,25°C,5s	73.1865	0.1mm
Softening point	>98	°C
Degree of delay,5°C,5cm/min	37.3485	cm
Dynamic viscosity (60°C)	335155	Pa·s
Kinetic viscosity (135°C)	4.7988	Pa·s

4. Characterization of fine structure of construction asphalt mixtures

4.1. *Shape characteristics*

Table 4 shows the results of the mean, standard deviation, and coefficient of variation (COV) of each parameter for the three aggregates.The index values of two-dimensional shape, sphericity, angle of gradient, and flattening ratio of the three aggregates are similar, and all the fine aggregates are semi-elongated, while the values of sphericity of the coarse aggregates are all lower, and the coarse and fine aggregates are rounded. While the surface texture index value varies greatly, the number of particles of granite, gneiss as well as rattlesnake are 406, 519 and 653 respectively, and the roughness of the three types of aggregates is in the trend of low, medium and high. Therefore, with similar production processes, the respective shape characteristics of the aggregates and the AIMS classification results were similar except for texture, which was not affected by the mineral composition of the aggregates. While texture was the only characteristic that contributed to the different classifications of the three aggregates, rattlesnake aggregate had a rough surface while granite had a smooth surface.

Table 4. The mean, standard deviation and variation coefficient of the parameters

Attribute	Mineral composition	Mean	Grain quantity	Standard deviation	COV /%	Categories
The fine aggregate is two-dimensional	Granite	8.4562	3654	2.2456	26.5152	Semi-elongation
	Cerite	8.3985	4563	2.3315	27.0485	
	Sounding rock	8.4687	5498	2.2648	26.3123	
Coarse aggregate ball	Granite	0.63	395	0.1152	17.49	Low

		53			85	sphericity
	Cerite	0.6753	694	0.1065	14.9648	
	Sounding rock	0.7165	596	0.0985	12.8635	
Aggregate gradient Angle	Granite	3798	4062	1279	35	Roundness
	Cerite	3627	5215	1265	36	
	Sounding rock	3336	6135	948	30	
Coarse aggregate surface texture	Granite	284.7966	406	107.4968	37.3568	Low roughness
	Cerite	328.8485	519	212.4968	55.2645	Medium roughness
	Sounding rock	562.1348	653	124.4688	22.1688	High roughness
Coarse aggregate flat ratio	Granite	2.9645	397	1.1358		-
	Cerite	2.5489	695	0.9285	36.8485	
	Sounding rock	2.3489	600	0.7856	30.4268	

4.2. Angularity characteristics

4.2.1. Limestone aggregate angularity measurement results and analysis. The mean (μ) and standard deviation (σ) of the six grades of limestone grain size aggregates are shown in the data in Table 5, and it can be observed that the angularity parameters of each grade of limestone aggregates have small standard deviation σ values ranging from 0.0325 to 0.0548, which suggests that the angularity parameter of the aggregates has a small degree of discretization and the data distribution is relatively stable. Since the focus of this paper is on prismaticity, the standard deviation's will not be discussed too much. Among them, the third standard cave slag limestone has the largest prismatic parameter, and the prismatic parameter in all six grades of grain size is above 1.1.

Table 5. Limestone angular parameters

Material source	Normal parameter	Aggregate size (mm)					
		2.36~4.75	4.75~9.5	9.5~13.2	13.2~16	16~19	19~26.5
Zibo flood spring	μ	1.0585	1.0785	1.0875	1.0846	1.1045	1.1064
	σ	0.0348	0.0455	0.0423	0.0348	0.0426	0.0348
Two hole slag	μ	1.0315	1.0866	1.0846	1.0978	1.0897	1.0978
	σ	0.0423	0.0456	0.0348	0.0435	0.0325	0.0348
Three hole slag	μ	1.1348	1.1136	1.1265	1.1348	1.1648	1.1348
	σ	0.0348	0.0489	0.0548	0.0348	0.0433	0.0486

Linqu Johnson(Stone)	μ	1.0625	1.0879	1.0987	1.0879	1.0978	1.1056
	σ	0.0378	0.0365	0.0365	0.0465	0.0342	0.0463

4.2.2. Basalt aggregate angularity measurement results and analysis. The mean (μ) and standard deviation (σ) of the three grades of basalt grain size aggregates are shown in Table 6. By analyzing the data on the angularity characteristics of basalt, it can be observed that in the range of grain sizes from 4.75 mm to 9.5 mm, from 9.5 mm to 13.2 mm, and from 13.2 mm to 16 mm, the differences of the Chifengxiangyodi, Jinanxing'an and Jusen basalts of Linqu are not significant in terms of angularity parameters. The difference in the parameters is not significant, and the mean value of all aggregate grain size is 1.0887. This phenomenon can be explained from two aspects, the material source characteristics and processing characteristics of basalt.

Firstly, from the viewpoint of source properties, all three basalts have excellent mechanical properties. Secondly, from the processing characteristics, Chifeng Xiangyodi basalt, Jinan Xing'an basalt and Linqu Jusen basalt all adopt secondary crushing process in the production process. Because of their similarity in rock properties and crushing process, they show high similarity in aggregate angularity.

Table 6. The angular characteristics of the basalt collection

Material source	Normal parameter	Aggregate particle size (mm)		
		4.75~9.5	9.5~13.2	13.2~16
Chifeng township about land	μ	1.0798	1.0846	1.0846
	σ	0.0348	0.0355	0.0366
Xingan City of Jinan	μ	1.0886	1.0879	1.0978
	σ	0.0485	0.0346	0.0426
Linqu Jusen (Xuan)	μ	1.0896	1.0978	1.0875
	σ	0.0364	0.0436	0.0346

4.3. Distributional characteristics

Calculate the trend of aggregate inclination of five kinds of mixtures to obtain the trend of aggregate inclination when the mixture reaches a stable state, the results are expressed in the form of the average inclination of all the coarse aggregates in the cross-section, and the calculation results are shown in Table 7, five kinds of asphalt mixtures have already reached a stable state in the early stage of compaction, and there is a fluctuation range of ±2.15° of the average inclination of the aggregate under different compaction times, and there is not a good linear relationship between the number of times and inclination of the asphalt mixture. There is no good linear relationship between the number of times of compaction and the angle of inclination.

Table 7. Aggregate average inclination calculation result(°)

Class type	Compaction number(Frequency)								
	25	50	75	100	150	200	300	500	1000
GAC	38.2975	37.8656	39.1648	37.7625	39.8032	38.7923	39.5576	38.7268	39.7034
SUPERPAVE	41.9663	41.7662	39.4822	40.9422	40.4321	41.9536	40.5132	38.7126	39.8723
SAC	41.2798	40.0378	38.5063	41.8369	40.2366	39.3485	40.4636	39.4325	39.9612
SMA	40.1064	41.1988	40.1645	39.3648	40.2431	39.4956	40.4123	41.5433	40.1536
OGFC	34.9785	35.6315	38.2648	39.4346	36.7985	36.0248	36.9648	38.0536	36.7269

Under the action of load, the aggregate particles occur in addition to the occurrence of translation, but also produce rotation. The angle of inclination is the angle between the main axis and the horizontal x-axis, reflecting the rotation of the aggregate particles under the action of the load, and can be used as a statistical index to reflect the rotation of the aggregate particles. The smaller the inclination angle, the closer the main axis of the aggregate particles is to the horizontal, i.e., the aggregate particles are "overwhelmed". In addition to the angle of rotation of the aggregate, the angle of radiation can also reflect the changes in the translational position of the aggregate particles. If the aggregate particles do not rotate under the action of the load, but only produce a small flat movement. Then the particle downward and leftward advection, the radiation angle becomes smaller, and the particle upward and rightward advection, the radiation angle increases. Figure 4 shows three different asphalt mixtures, in the load effect of each stage of the inclination angle and radiation angle change curve, Figure (a) for the SMA inclination angle trend, Figure (b) for the SMA radiation angle trend, Figure (c) for the rock asphalt, SAC-16 inclination angle trend, Figure (d) for the rock asphalt, SAC-16 radiation angle trend, Figure (e) for the 70 # asphalt, OGFC inclination angle change trend , Figure (f) shows 70# asphalt, OGFC radiation angle trend.

The distribution of the initial inclination and radiation angle of aggregate particles generally shows the law of "less quantity of aggregate in the middle angle and more quantity of aggregate in the two ends angle", which indicates that the main axis of most of the aggregate particles is close to the horizontal state, but there are still some aggregate particles whose main axes are close to 90º. With the continuous action of the load, the asphalt mixture is gradually compacted, the number of aggregates with inclination and radiation angles of 45º~135º decreases, while the number of aggregates with inclination and radiation angles of 0º~45º and 135º~180º increases, which indicates that the main axes of the aggregate particles are close to the horizontal state. Taking the asphalt mixture of SMA as an example, its frequency of aggregates with inclination and radiation angles of 45º~135º ranged from 1.897% to 5.345% and 1.208% to 5.199% when loaded for 3 h. The frequency of aggregates with inclination and radiation angles of 0º~45º and 135º~180º increased continuously, indicating that the main axis of the aggregate particles was constantly approaching the horizontal state. The highest aggregate frequency for inclination and radiation angles of 0º~45º and 135º~180º were 11.348% and 14.02% respectively. The trends of inclination and radiation angles for the above three asphalt mixtures at all stages are consistent and differ only in the magnitude of change.

The inclination angle reflects the changes caused by the rotation of the main axis of the aggregate particles, while the radiation angle not only reflects the changes in the rotation angle of the aggregate particles, but also reflects the changes in the displacement of the center of gravity due to the generation of translational movement of the aggregate particles. Since the wheels carried out grinding back and forth during the experiment, it can be assumed that a large number of aggregate particles have the same probability of generating translational movement to the left and to the right, and some of the aggregate particles will generate vertical downward displacement, resulting in a smaller radiation angle.

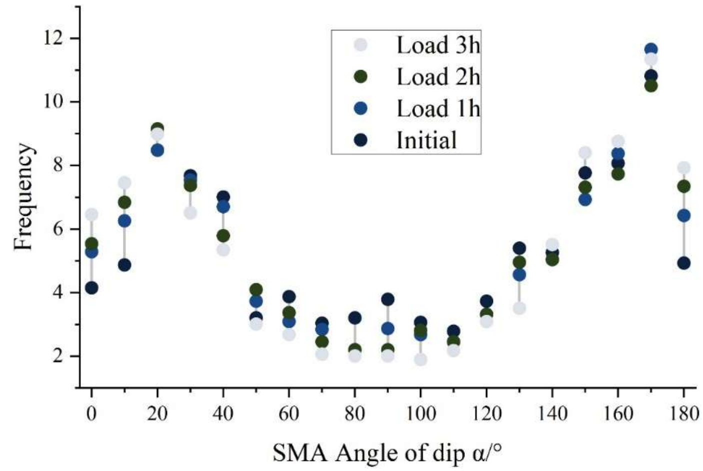

(a)SMA dip trend

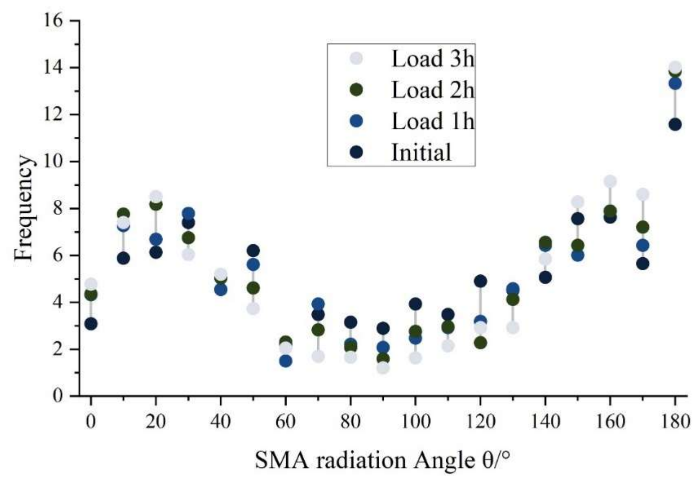

(b)Variation trend of SMA radiation Angle

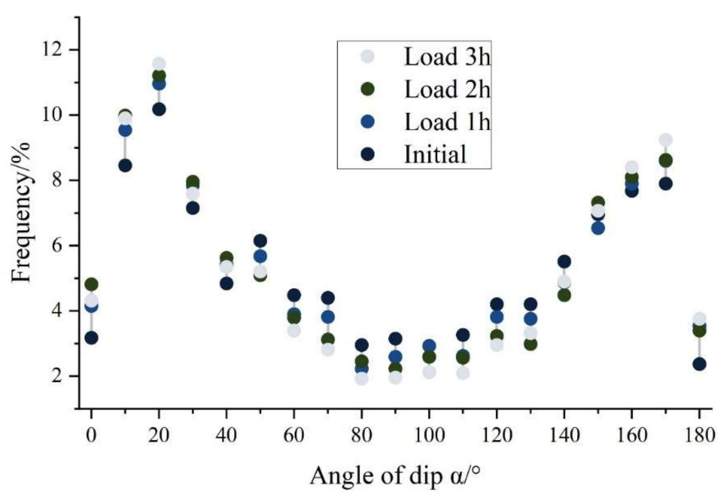

(c)Rock asphalt, SAC-16 Angle change trend

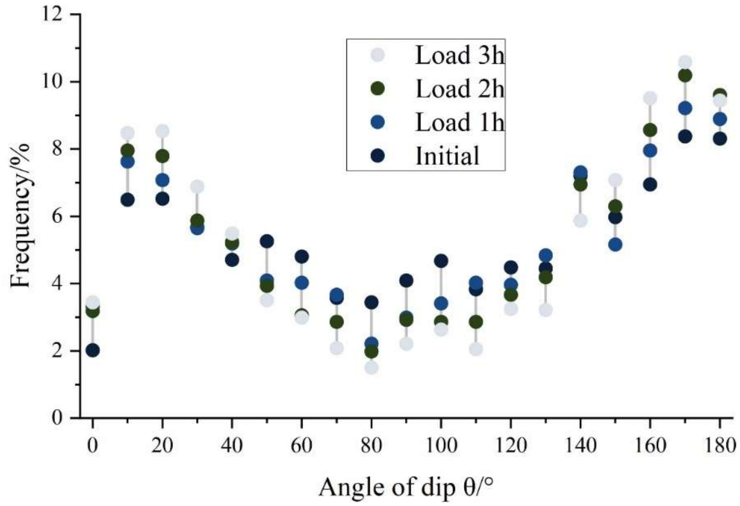

(d)The trend of rock asphalt, SAC-16 radiation Angle

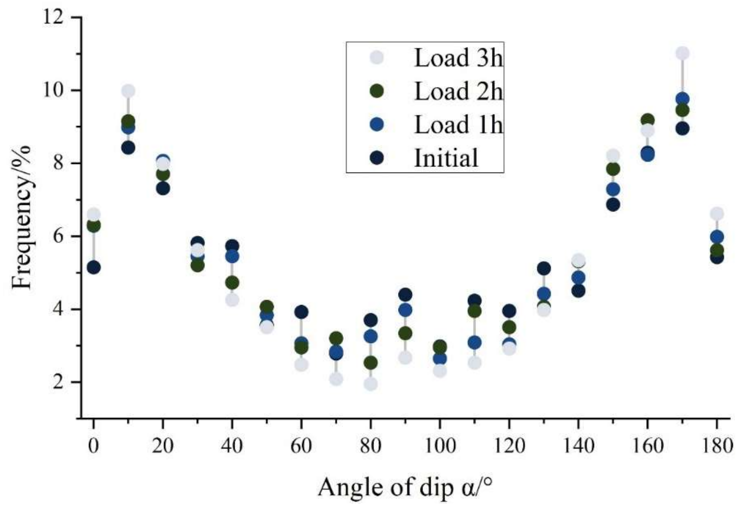

(e)70 # asphalt and OGFC dip trend

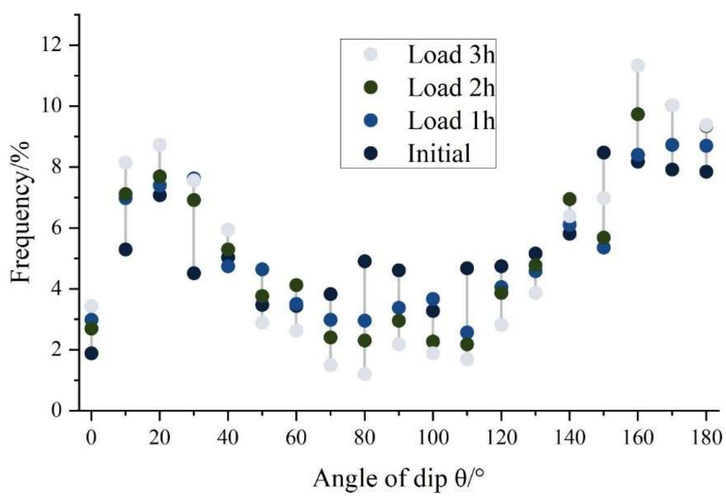

(f)70 # asphalt and OGFC radiation Angle change trend

Fig. 4. Distribution of inclination and radiation angle at each loading stages

4.4. Asphalt Mixture Contact Fine Structure Characterization and Uniformity Evaluation

In this study, the contact characteristics and uniformity of the fine structure of asphalt mixtures will be evaluated by establishing a coarse aggregate contact model with Voronoi diagrams, which will investigate the characteristics of asphalt mixtures in terms of the following five aspects: uniformity, coarse aggregate embedding relationship, and the distribution of aggregate contacts.

4.4.1. Distributional Characteristics of Coarse Aggregate Contact Voronoi Plots. Voronoi diagram, as a comprehensive and objective tool for measuring spatial proximity, was applied in this study to represent the spatial relationships between the contact points of asphalt mixture skeletons and to construct a contact model of the skeleton structure. Important data information is extracted from this model to evaluate the skeleton contact characteristics of different gradation.

In order to further analyze quantitatively, the method of quantitative statistics on the area of Voronoi polygon is adopted, and the area range is divided into different zones with a group spacing of 30 mm^2: 0-30 mm^2, 30-60 mm^2, 60-90 mm^2, 90-120 mm^2, 120-150 mm^2, 150-180 mm^2, 180-210 mm^2 and so on. With these statistical results, the Voronoi area distribution graphs were obtained as shown in Fig. 5, and Fig. (a)-Fig. (d) represent the contact area of gradation 1-4, respectively. The area distribution of the contact Voronoi diagrams for asphalt mixture skeletons with different gradation is demonstrated.

Combined with the nature of Voronoi polygon, the following conclusions can be drawn:

1) The area of the Voronoi diagrams at the aggregate contact points is normally distributed, and the area of the Voronoi diagrams generated by the four gradings is larger in the range of 30-180 mm^2. The finer the gradation, the smaller the percentage of this area. The results show that G1 accounts for 66.67%, G2 accounts for 68.52%, G3 accounts for 80.3%, and G4 accounts for 93.55%.

2) The finer the gradation, the greater the proportion of the generated Voronoi area in the range of the interval greater than 180 mm^2. Among them, grade 1 accounts for 33.33%, grade 2 accounts for 31.48%, grade 3 accounts for 19.7%, and grade 4 accounts for 6.45%. The Voronoi diagrams with larger area are distributed at the edge of the asphalt mixture specimens.

3) The larger the area of the Voronoi diagram, the farther the corresponding skeleton contact point is from other contact points. Therefore, the larger the area of the Voronoi diagram in the image, the more discrete the distribution of the skeleton contact points of the graded mixture, the more unfavorable to the formation of the skeleton contact force chain.

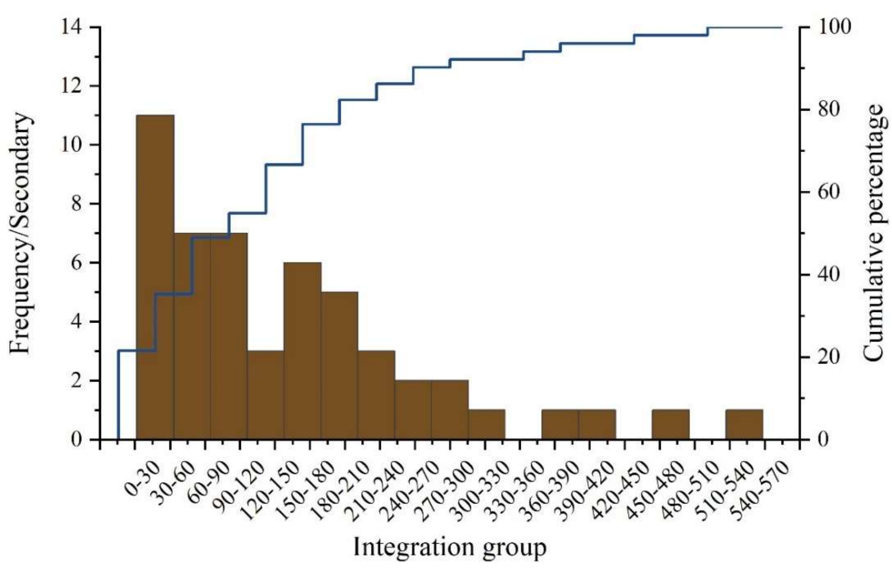

(a)Gradation 1

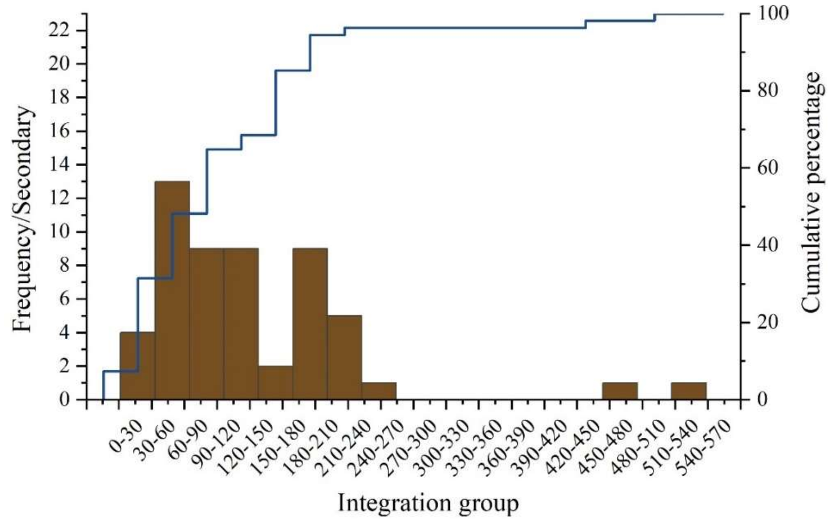

(b)Gradation 2

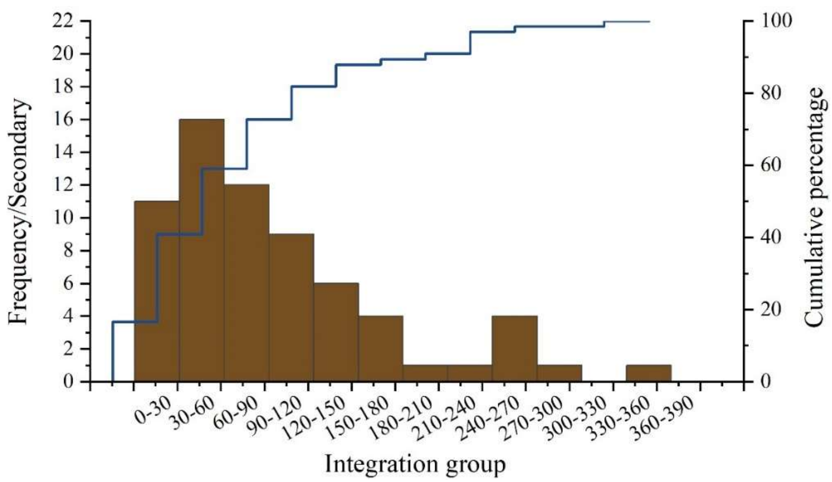

(c)Gradation 3

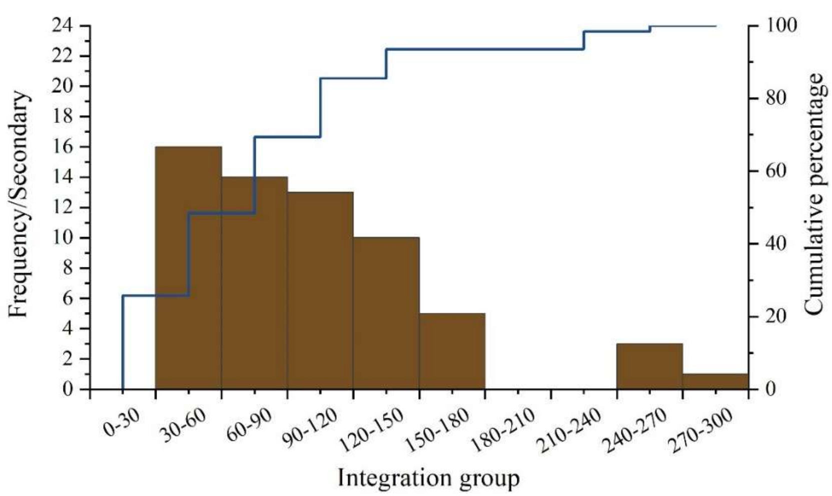

(d)Gradation 4

Fig. 5. Voronoi area distribution

4.4.2. Distributional characteristics of contact connectivity trees for asphalt mixtures. A graph that is connected and contains no loops is called a tree in discrete mathematics. In this paper, the CT image processing algorithm is utilized to identify the fine structure of asphalt mixtures, and the resulting connected coarse aggregate group diagram is called a connected tree Figure 6 shows the distribution of connected trees. The connected tree is composed of the center points of the coarse aggregates that are in contact with each other and connected to a piece, and the nodes of the connected tree (i.e., the center points of the coarse aggregates) are specified to be the order of the tree. A tree with n nodes is called an n-order tree and is defined as a 2-order tree as the first-order tree noted as Tr-1, a 3-4-order tree as the middle-order tree noted as Tr-2, and a 5-order and above as the higher-order tree noted as Tr-3.The distributional characteristics of the connectivity trees for coarse aggregate contact are investigated by analyzing the statistics of the number and order of the connectivity trees generated by each level of the graded matches. The number of connectivity trees is higher for gradation 1 and gradation 2, and the number of connectivity trees is lower for gradation 3 and gradation 4. Among the four grades, Grade 1 has the significantly highest number of primitive trees, and Grade 4 has the lowest number of higher-order trees. The results show that the number of connecting trees has no obvious correlation with the skeleton contact characteristics, and is not suitable as an evaluation index of skeleton contact characteristics. The proportion of primary and middle-order trees in grade 1 is 61.54%, grade 2 is 92.31%, grade 3 is 83.33%, and grade 4 is 58.82%. Among them, the higher the proportion of the first-order tree, especially the higher the proportion of the second-order tree, indicating that the worse the skeleton contact connectivity, the coarse aggregates did not form a good embedded relationship, the more unfavorable to the improvement of the shear strength of asphalt mixtures.

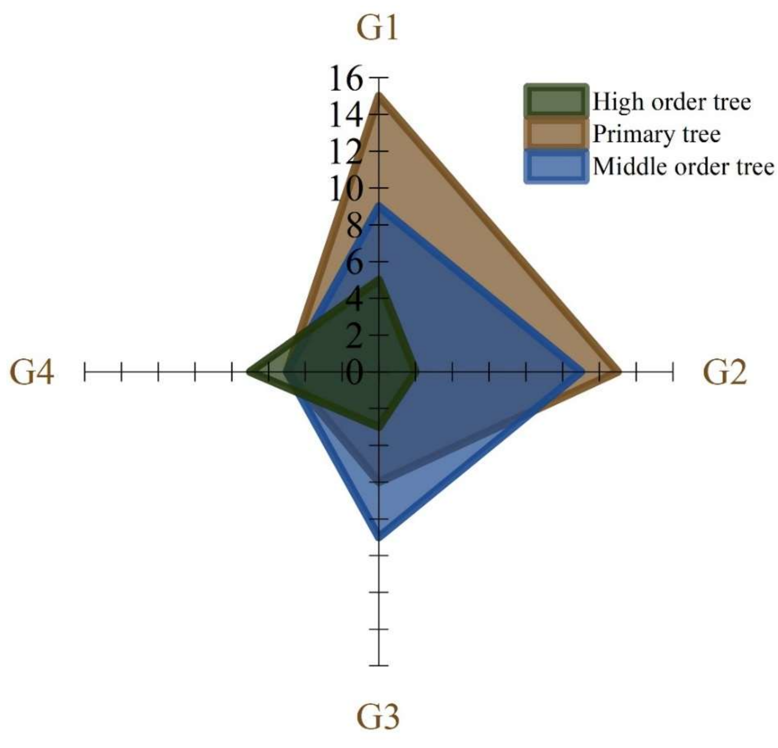

Fig. 6. Connected tree distribution

4.4.3. Area Evaluation of Contact Connectivity Trees for Voronoi diagrams. The sliced images of the specimens with four different grades were statistically analyzed to determine the areas of the trees of each order. The sum of the generated Voronoi polygon areas corresponding to the skeleton contact points contained in the connectivity tree is defined as the area of the tree, which is denoted as the connectivity tree area TVs.The statistical results of the connectivity tree areas for each level of specimen are shown in Fig. 7. The distribution of the area of each order tree for each level of allocation is shown in Fig. 8, Fig. 8(a) shows the number of initial order, Fig. 8(b) shows the middle order tree, and Fig. 8(c) shows the high order tree.

1) Most of the area of the primary order trees is distributed between 100 mm^2-300 mm^2, the area of the middle order trees is basically distributed between 200 mm^2-400 mm^2, while the distribution of the high order trees is between 400 mm^2-500 mm^2.

2) The connected tree area TVs are basically distributed within 500 mm^2. Among them, about 84.91% of TVs values of Grade 1 and Grade 2 are distributed within 500, and about 74.29% of TVs values of Grade 3 and Grade 4 are distributed within 500. It indicates that gradation 1 and gradation 2 contain very few higher-order trees, and the skeleton connectivity is relatively weak.

3) 12.43% and 16.52% of the data in the area of the first-order trees of Grade Match 1 and Grade Match 2, respectively, show a large discrepancy, indicating that the contact points corresponding to this part of the tree are far away from the other contact points and are relatively discrete. Twenty-two percent of the data in the area of the higher-order tree of level match 3 showed a large difference, indicating that this part of the tree has a larger order and the connectivity strength of this tree is large. However, the content of high-order tree of Grade 3 is not high, which laterally indicates that a part of the skeleton contact of Grade 3 is very good, and the rest of the skeleton contact performs average, and overall, the distribution of coarse aggregate contact is not homogeneous. The area distribution of higher-order trees of gradation 4 is more uniform and concentrated, reflecting that the connecting strength of connecting trees of gradation 4 is basically the same, and the aggregate contact is uniformly distributed, with better load transfer chain and rutting resistance.

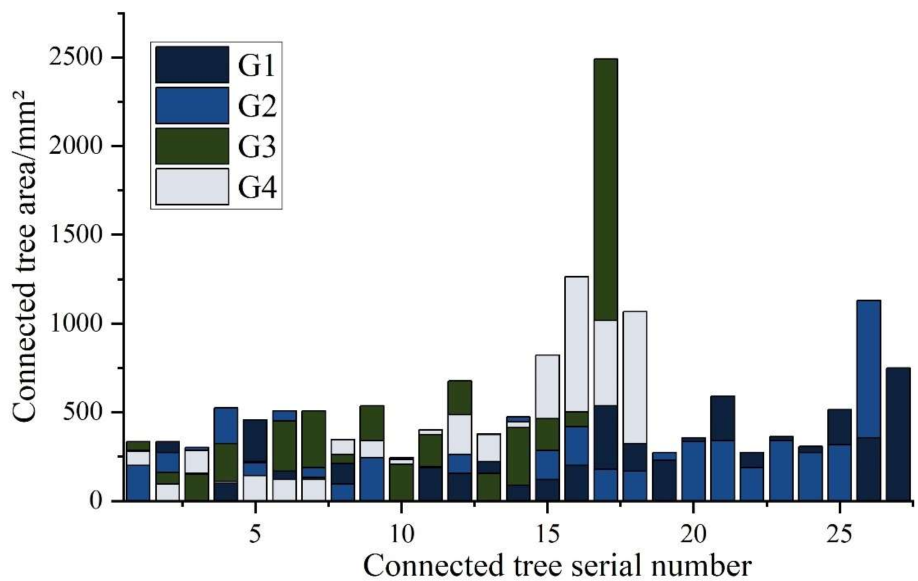

Fig. 7. Area distribution of connected trees

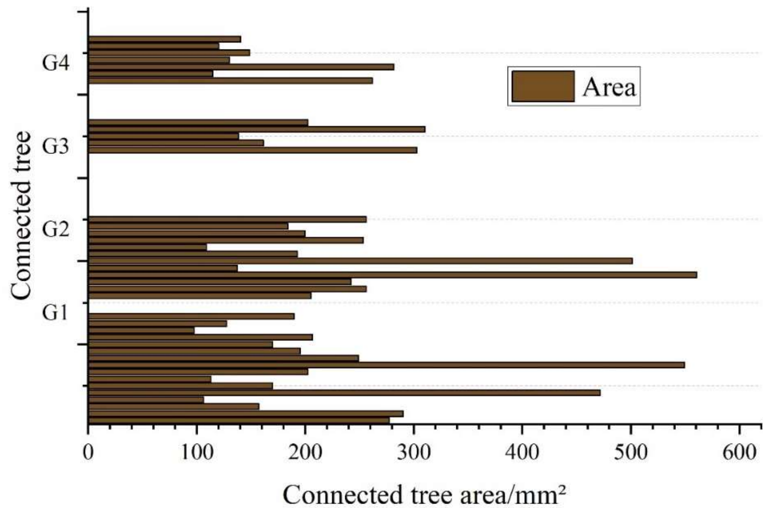

(a)First order tree

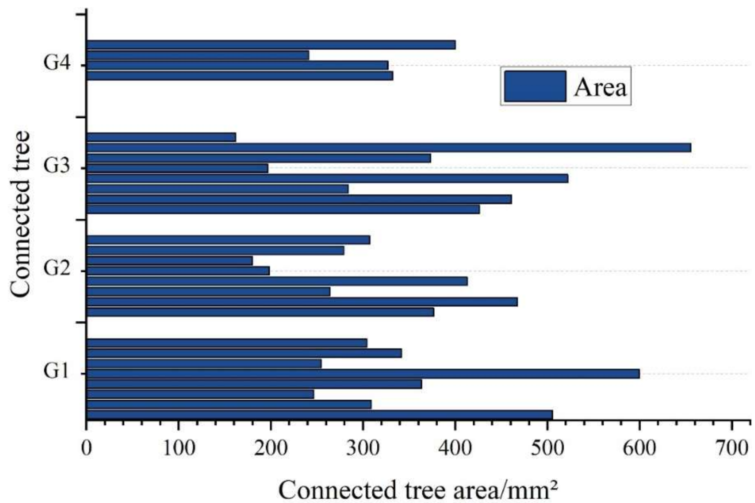

(b)Middle tree

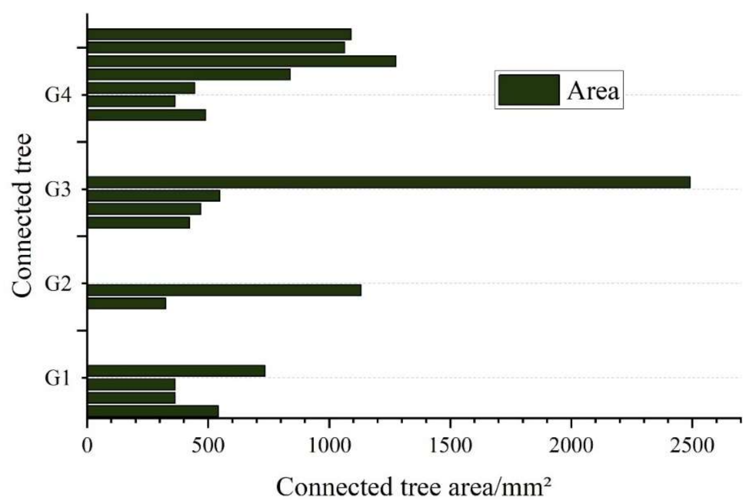

(c)High order tree

Fig. 8. Area distribution of trees of each order

4.4.4. Homogeneity evaluation. The rutting resistance of asphalt mixtures is an important index for assessing their road performance, which mainly depends on the bonding and embedding ability between coarse aggregates and the uniformity of aggregate distribution. In order to study the road performance of asphalt mixtures in depth, this section compares and analyzes it from two perspectives: macroscopic and microscopic. In the macro aspect, two mechanical indexes, dynamic stability (DS) and rutting depth (RD), are used to characterize the rutting resistance of asphalt mixtures. According to the test protocol (JTG E20-2011), four groups of graded specimens were tested for rutting to obtain DS and RD values, and these macroscopic indexes can directly reflect the deformation and damage of asphalt mixtures under stress. On the detailed side, this paper proposes seven characteristic parameters of the skeleton contact structure: Voronoi diagram area Vs, Voronoi diagram number Vc value, connecting tree number Tc value, connecting tree order n value, connecting tree area TVs, contact point length C_1, total length of the contact points L. To analyze the distribution of the variability of the detailed parameters of the different grades, the statistical parameters adopted include maximum value, minimum value, median, mean, standard deviation and coefficient of variation. The statistical results are shown in Tables 8 and 9.

1) Dynamic stability: Grade 1 (1876) <Grade 2 (1966) <Grade 3 (2164) <Grade 4 (3048), rutting depth: Grade 1 (6.35) >Grade 2 (5.86) >Grade 3 (3.64) >Grade 4 (2.98), which indicates that the rutting resistance of Grade 1 is very poor, that the rutting resistance of Grade 2 is poor, and that the rutting resistance of Grade 3 is average. Gradation 4 has better rutting resistance. There is a clear relationship between dynamic stability and rutting depth.

2) The contact length between aggregates is an important parameter reflecting the effectiveness of aggregate contact. The total contact length: grade 1<grade 2<grade 3<grade 4 is 27.23mm, 42.36mm, 71.36mm and 90.64mm respectively, and the average value of contact length: grade 1<grade 2<grade 3<grade 4. It can be analyzed that, the total contact length of grade 1 is the smallest and the average value is the smallest, which indicates that the aggregate contact effectiveness of grade 1 is the worst, and the total contact length and average value of grade 4 are both the largest, reflecting that it has better rutting resistance than grade 4, and that its rutting depth is better. The total contact length and average value of gradation 4 are the largest, reflecting that it has the best contact effect.

3) With the finer gradation, the smaller standard deviation and coefficient of variation of Voronoi diagram area are, reflecting that gradation 4 aggregate contact points are less discrete and uniformly distributed, and the relative performance of gradation 1 aggregate contact characteristics is the worst.

Table 8. Macroscopic and mesoscopic parameters of asphalt mixture

Grading type	Mesoscopic index				Macro index	
	Voronoi diagram quantity Vc	Number of connected trees Tc	Contact length L/mm	Voronoi Total area/mm^2	RD/ mm	DS times· mm^{-1}
G1	54	28	27.2954	8075.6485	6.3485	1876
G2	56	25	42.3648	8154.7856	5.8645	1966
G3	67	18	71.3648	8064.2165	3.6436	2164
G4	80	17	90.6351	7982.6655	2.9785	3048

Table 9. Distribution variability of mesoscopic parameters

Detail parameter	Class type	Maximum value	Minimum value	Median	Mean value	Standard deviation	Variation coefficient
Connected tree number n value	G1	7.1325	2.1542	2.1542	2.8468	1.3248	0.4688
	G2	13.4666	2.0486	3.0486	3.4456	2.1165	0.7054
	G3	26.4568	2.0485	3.0436	4.5488	5.5698	1.2478
	G4	14.0486	2.0398	4.0156	4.9785	3.7648	0.7642
Contact length C1	G1	0.5798	0.5268	0.5435	0.5464	0.0154	0.0265
	G2	4.6456	0.1645	0.4168	0.7845	0.8546	1.0846
	G3	8.3488	0.1652	0.7458	1.1345	1.2188	1.1054
	G4	6.5488	0.1658	0.5599	1.1566	1.2789	1.1048
Connected tree area	G1	728.4856	93.4556	245.4855	294.5748	165.0486	0.5432
	G2	1113.4856	105.4854	264.4688	313.4685	198.4625	0.6123
	G3	2487.4838	137.8756	374.1685	475.6458	525.6755	1.1026
	G4	1287.6456	112.4669	329.4644	440.3165	348.3466	0.7856
Voronoi Surface product	G1	553.6554	24.5315	118.7648	155.2448	108.5516	0.6487
	G2	564.1352	43.4315	130.4687	151.6486	96.4361	0.6315
	G3	375.9485	22.6787	110.7895	124.0685	74.4648	0.6136
	G4	282.3946	17.0548	91.0846	100.2987	58.4874	0.5848

5. Conclusion

In this paper, the three-dimensional reconstruction of asphalt mixtures is realized by using X-ray CT technology through the trinomialization operation of asphalt mixture tomographic images and optimized image processing. The three-dimensional fine structure characterization indexes of asphalt mixtures are proposed, the gradation of asphalt mixtures is designed, and the specimens for structural characterization are prepared. The number of shaped particles in the tested aggregates, granite, gneiss as well as rattlesnake are 406, 519 and 653 respectively, and the roughness of the three aggregates tends to be low, medium and high. The percentage of Voronoi diagram area generated by the four grades between 30-180 mm^2 is relatively large, and the percentage of G1, G2, G3, and G4 grades are 66.67%, 68.52%, 80.3%, and 93.55%, respectively. In the uniformity evaluation, the total length of contact points of grades 1~4 were 27.23 mm, 42.36 mm, 71.36 mm and 90.64 mm, respectively, and the two statistical parameters of total contact length and average value of grade 4 were the largest, reflecting its best contact effect and better uniformity.

References

[1] Feng, B., Wang, H., Li, S., Ji, K., Li, L., & Xiong, R. (2022). The durability of asphalt mixture with the action of salt erosion: A review. Construction and Building Materials, 315, 125749.

[2] Zhang, M., Hao, P., Men, G., Liu, N., & Yuan, G. (2021). Research on the compatibility of waterproof layer materials and asphalt mixture for steel bridge deck. Construction and Building Materials, 269, 121346.

[3] Yang, L., Tao, L., Hai, W., Rui, L., Jianzhong, P., & Zhibin, F. (2024). Safety and comfort evaluation of high-speed cycling on urban asphalt pavement. Transportation research record, 2678(7), 622-641.

[4] Tabasi, E., Zarei, M., Mobasheri, Z., Naseri, A., Ghafourian, H., & Khordehbinan, M. W. (2023). Pre-and post-cracking behavior of asphalt mixtures under modes I and III at low and intermediate temperatures. Theoretical and Applied Fracture Mechanics, 124, 103826.

[5] Meng, Y., Liu, D., Rong, H., & Yang, X. (2024). Review and prospect of four-point bending fatigue test of asphalt mixture. Journal of Road Engineering.

[6] Wang, Y. D., Liu, J., & Liu, J. (2023). Integrating quality assurance in balance mix designs for durable asphalt mixtures: State-of-the-art literature review. Journal of Transportation Engineering, Part B: Pavements, 149(1), 03122004.

[7] Imjai, T., Garcia, R., Rassameekobkul, W., Sofri, L. A., & Wicaksono, A. (2024). Service Performance of Porous Asphalt Mixtures in Thailand: Laboratory and Full-Scale Field Tests. International Journal of Pavement Research and Technology, 1-18.

[8] Niu, D., Xie, X., Zhang, Z., Niu, Y., & Yang, Z. (2021). Influence of binary waste mixtures on road performance of asphalt and asphalt mixture. Journal of Cleaner Production, 298, 126842.

[9] Li, X., Shi, L., Liao, W., Wang, Y., & Nie, W. (2024). Study on the influence of coarse aggregate morphology on the meso-mechanical properties of asphalt mixtures using discrete element method. Construction and Building Materials, 426, 136252.

[10] Hassan, H. M. Z., Wu, K., Huang, W., Chen, S., Zhang, Q., Xie, J., & Cai, X. (2021). Study on the influence of aggregate strength and shape on the performance of asphalt mixture. Construction and Building Materials, 294, 123599.

[11] Sun, C., Li, P., Xu, Y., Ma, Y., & Niu, B. (2024). Structure evolution analysis of asphalt mixtures during compaction based on particle tracking and granular properties. Construction and Building Materials, 425, 136089.

[12] Gao, L., Zhang, Y., Liu, Y., Wang, Z., & Ji, X. (2023). Study on the cracking behavior of asphalt mixture by discrete element modeling with real aggregate morphology. Construction and Building Materials, 368, 130406.

[13] Huang, G., Chen, Z., Wang, S., Hu, D., Zhang, J., & Pei, J. (2024). Investigation of fracture failure and water damage behavior of asphalt mixtures and their correlation with asphalt-aggregate bonding performance. Construction and Building Materials, 449, 138352.

[14] Yu, H., Zhou, S., Qian, G., Zhang, C., Shi, C., Yao, D., & Ge, J. (2023). Evaluation of the microscale structure and performance of asphalt mixtures under different design methods. Construction and Building Materials, 400, 132810.

[15] Liu, Z., Sun, L., Zhai, J., & Huang, W. (2022). A review of design methods for cold in-place recycling asphalt mixtures: Design processes, key parameters, and evaluation. Journal of Cleaner Production, 370, 133530.

[16] Sun, J., Zhang, H., Liu, D., Yu, M., Lv, R., & Liu, Y. (2024). Micro-structural characteristics of asphalt

mixture and its effect to mechanical performance based on two-stage mixing method. Construction and Building Materials, 411, 134258.

[17] Sun, C., Li, P., Ma, Y., Niu, B., Gou, X., & Tian, C. (2025). Shear failure in asphalt mixtures under torsional loading: Evaluation methods, failure mechanisms and evolution behavior. Construction and Building Materials, 462, 139979.

[18] Chen, Y., Xu, S., Tebaldi, G., & Romeo, E. (2022). Role of mineral filler in asphalt mixture. Road materials and pavement design, 23(2), 247-286.

[19] Awed, A. M., Tarbay, E. W., El-Badawy, S. M., & Azam, A. M. (2022). Performance characteristics of asphalt mixtures with industrial waste/by-product materials as mineral fillers under static and cyclic loading. Road Materials and Pavement Design, 23(2), 335-357.

[20] Shafabakhsh, G., Rahmani, A., & Sadeghnejad, M. (2022). Evaluation the Effect of Different Kind of Waste and Mineral Filler on the Fatigue Life of Asphalt Mixtures with Dissipated Energy Method. Journal of Rehabilitation in Civil Engineering, 10(2), 56-67.

[21] Ren, Z., Tan, Y., Huang, L., & Xiao, S. (2023). Fractal and multifractal characteristics of three-dimensional meso-structure for asphalt mixture. Construction and Building Materials, 384, 131429.

[22] Taheri-Shakib, J., & Al-Mayah, A. (2023). A review of microstructure characterization of asphalt mixtures using computed tomography imaging: Prospects for properties and phase determination. Construction and Building Materials, 385, 131419.

[23] Zhao, X., Niu, D., Zhang, P., Niu, Y., Xia, H., & Liu, P. (2022). Macro-meso multiscale analysis of asphalt concrete in different laboratory compaction methods and field compaction. Construction and Building Materials, 361, 129607.

[24] Gong, X., Jiang, Y., Ou, S., Qian, G., & Liu, Z. (2023). Characterization on the mesostructural distribution of asphalt mixtures via digital image processing and relation to macroscopic performances. Construction and Building Materials, 404, 133212.

[25] Taheri-Shakib Jaber & Al-Mayah Adil. (2023). A review of microstructure characterization of asphalt mixtures using computed tomography imaging: Prospects for properties and phase determination. Construction and Building Materials,385.

[26] Cheng Peng,Zhi chao Wang,Chong zheng Zhu & Du min Kuang. (2025). 3D reconstruction of asphalt mixture based on 2D images. Construction and Building Materials,462,139938-139938.

[27] Tao Huang & Guoqiang Liu. (2024). Evaluation for coarse aggregate distribution of asphalt mixtures based on the two-dimensional digital image analysis. Construction and Building Materials,450,138716-138716.